

Reciprocal Metasurfaces for On-axis Reflective Optical Computing

Ali Momeni, Hamid Rajabalipanah, Mahdi Rahmazadeh, Ali Abdolali*, Karim Achouri, Viktor Asadchy and Romain Fleury*.

Abstract—Analog computing has emerged as a promising candidate for real-time and parallel continuous data processing. This paper presents a reciprocal way for realizing asymmetric optical transfer functions (OTFs) in the reflection side of the on-axis processing channels. It is rigorously demonstrated that the presence of Cross-polarization Exciting Normal Polarizabilities (CPENP) of a reciprocal metasurface circumvents the famous challenge of Green’s function approach in implementation of on-axis reflective optical signal processing while providing dual computing channels under orthogonal polarizations. Following a comprehensive theoretical discussion and as a proof of concept, an all-dielectric optical metasurface is elaborately designed to exhibit the desired surface polarizabilities, thereby reflecting the first derivative and extracting the edges of images impinging from normal direction. The proposed study offers a flexible design method for on-axis metasurface-based optical signal processing and also, dramatically facilitates the experimental setup required for ultrafast analog computation and image processing.

Index Terms—Optical Signal Processing, all-dielectric Metasurfaces, Surface Polarizabilities.

I. INTRODUCTION

OVER the past few years, the growing demands for ultrafast and large-scale signal, image, and information system processing as well as the saturation of digital computational capacities have brought about the emergence of new proposals for optical analog computing schemes [1]–[3]. In traditional approaches, mathematical processing is mainly performed in the digital domain by using traditional integrated electronic-based technologies for implementing logics [4]–[7], differentiators and integrators [8], [9]. Unfortunately, these computing hardwares have some major disadvantages related to operational speed and power consumption [10], [11]. Recently, Silva *et. al* [11] have proposed the construction of analog computational metamaterials, based on two distinct approaches: the spatial Fourier transfer and Green’s function (GF) methods [12]. The former solution, executed

in the spatial Fourier domain, was initially accompanied with additional bulky optical components ($4f$ correlators), hindering miniaturization [11], [13]. This shortcoming was later avoided by directly realizing the spatial impulse response of interest by means of the nonlocal transmission or reflection response of artificial structures [14]–[17]. A large number of studies presented resonant and non-resonant structures to expand this idea for advanced all-optical signal processing architectures [18]–[20]. The authors in [15] have demonstrated that the nonlocality of artificial structures can be engineered to enable signal manipulation in the momentum domain over an ultrathin platform for performing basic mathematical operations in transmission mode. Another progress in this area, discussed in [14], has shown that the interference effects associated with surface plasmon excitations at a single metal-dielectric interface can perform spatial differentiation and edge detection. More recently, a theoretical work has demonstrated that the Laplacian operator required to do spatial differentiation in transmission mode can be obtained using the guided resonances of a photonic crystal slab [21]. Besides, different innovative approaches have been also reported, for instance manipulating the complex-valued electromagnetic wave propagating through specially designed recursive paths [22], or the use of topological insulators as a way to increase the robustness to geometrical tolerances [23].

In the GF-based optical signal processing methods, the metasurfaces often aim at realizing transfer functions (TF) with either odd-/or even-symmetric properties (see Fig. 1a). For odd/even TFs, the reflection or transmission coefficient of the metasurface processor should be an asymmetric/symmetric function of the incident angle. Due to fundamental limitations arising from the nonlocal behavior of reflection/transmission responses in the wavevector domain, the existing GF-based analog computing proposals have exploited complex oblique illumination setups (challenging to align) to implement odd-symmetric operations [14], [18], [19], [24], [25]. In most practical situations, realizing on-axis signal processing operators with asymmetric optical transfer functions (OTFs) is a key requirement for increasing the compatibility with standard image processing/recognition schemes, such as image sharpening and edge detection [17], [26]–[28]. In addition, reflection-type processing systems are superior to transmission-type ones in terms of compactness. Besides, although using both reflection and transmission channels of the metasurfaces would enhance the degrees of freedom for performing parallel processing, the on-axis reflective channels are still unavailable. The reason is attributed to the fact that realizing an odd-symmetric angular

A. Momeni and R. Fleury are with the Laboratory of Wave Engineering, School of Electrical Engineering, Swiss Federal Institute of Technology in Lausanne (EPFL), Lausanne, Switzerland.

H. Rajabalipanah and A. Abdolali are with Applied Electromagnetic Laboratory, School of Electrical Engineering, Iran University of Science and Technology, Tehran 1684613114, Iran.

M. Rahmazadeh is with Electrical Engineering Department, Sharif University of Technology, Tehran 11155-4363, Iran.

K. Achouri is with Nanophotonics and Metrology Laboratory, Swiss Federal Institute of Technology Lausanne (EPFL), 1015 Lausanne, Switzerland.

V. S. Asadchy is with Ginzton Laboratory and Department of Electrical Engineering, Stanford University, Stanford, California 94305, USA, and also with the Department of Electronics and Nanoengineering, Aalto University, 00076 Aalto, Finland.

Corresponding authors’ emails: romain.fleury@epfl.ch and abdolali@iust.ac.ir

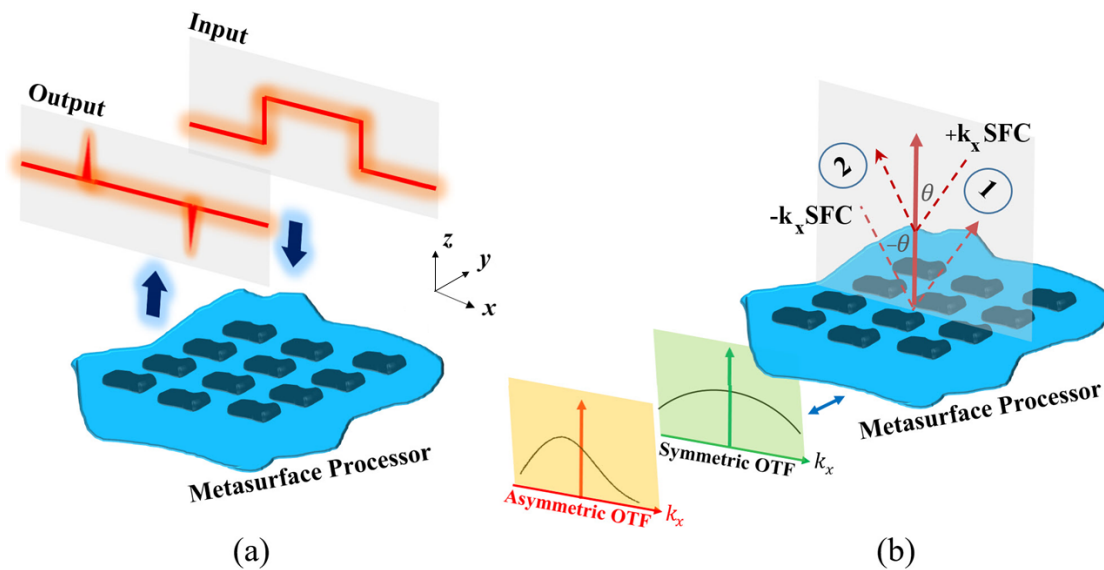


Fig. 1. (a) Schematic sketch of the proposed spatial metasurface processor for performing real-time on-axis reflective analog signal processing (b) Demonstration of the symmetries/asymmetries of the angular scattering around the boresight direction for nonreciprocal/reciprocal metasurfaces.

dispersion for co-polarized components of these channels violates the well-known reciprocity theorem [29]. Nevertheless, up to now prior proposals for accomplishing on-axis optical signal processing have only considered transmissive configurations [15], [26], [28]–[32].

Motivated by such theoretical developments, here, we propose a reciprocal way for exploiting the on-axis reflective processing channels in bianisotropic metasurfaces. We demonstrate that taking into account the cross-polarization reflections caused by the normal polarizabilities of bianisotropic metasurfaces brings in new degrees of freedom in controlling the meta-atom scattering. We reveal a simple appealing opportunity to circumvent the coercive reflection symmetry in the wavevector domain without resorting to intricate non-reciprocal options or bulky Fourier lenses. We show that using the cross-polarized channels enabled by a certain group of normal polarizabilities, the odd-symmetric operations can be implemented in on-axis reflective scenarios. Compared with recent works [26], [29], [31], [33], the main contributions of this paper are:

- 1) By considering the general form of the surface polarizabilities of a reciprocal bianisotropic metasurface, we extract the general rules for performing standard on-axis optical signal processing tasks in the reflection side. Some remarks about the transmission configuration are also presented.
- 2) Realizing an all-dielectric optical metasurface that exposes the desired collective polarizabilities and creates a cross-polarized reflective processing channel.

II. THEORETICAL INVESTIGATION

A. Scattering coefficients of a metasurface

Fig. 1a illustrates the employed computational metasurface comprising a uniform array of polarizable meta-atoms in the x - y plane ($z=0$). Let us consider that p -polarized (or s -polarized) light with a transverse field-profile of $s_{in}(x)$ impinges normally on the metasurface processor (along the

$-z$ direction). This incident light is reflected by the metasurface with a beam-profile $s_{out}(x)$ in the $+z$ direction. Here, p - and s -polarized refer to the polarized lights whose electric field is oriented along x and y directions, respectively, at normal incidences. In the spatial Fourier domain, each beam profile can be spectrally represented by a superposition of plane waves, as spatial Fourier components (SPF), i.e., $s_{in}(x) = \int_{-W}^W \tilde{s}_{inc}(k_x) \exp(jk_z z + jk_x x) dk_x$, and $s_{out}(x) = \int_{-W}^W \tilde{H}(k_x) \tilde{s}_{inc}(k_x) \exp(-jk_z z + jk_x x) dk_x$. Here, W denotes the spatial bandwidth of the input signal and $k_x = k_0 \sin \theta$ specifies the x component of the wavenumber of the plane wave harmonic illuminating the metasurface with the incidence angle θ . Moreover, $\tilde{H}(k_x)$ refers to the transfer function describing an operator of choice, that we aim at synthesizing. Due to the sub-wavelength periodicity of the metasurface along the x direction, the tangential wave vector k_x must be continuous at the interface. Therefore, the incident plane wave with k_x only generates a reflected propagating plane wave with the same k_x . Furthermore, the beam-profile transformation between the incident and reflected lights can be spectrally described by using a spatially-dispersive transfer function representing the mathematical operator of interest, $\tilde{H}(k_x) = s_{out}(k_x)/s_{in}(k_x)$. Mathematically speaking, the k_x -dependency of the transfer function should be imparted by the angular response of the scattering parameter (reflection or transmission coefficient) of the employed metasurface [34]. It should be noted that the challenges accompanied with reflective optical signal processing of on-axis illuminations are more severe than those of transmissive configurations. For instance, designing asymmetric reflective OTFs by using co-polarization channels inherently requires non-reciprocity [29]. Although both reflection and transmission problems will be investigated, the focus of the paper is the reflection mode. In this case, the output field of the metasurface processor is

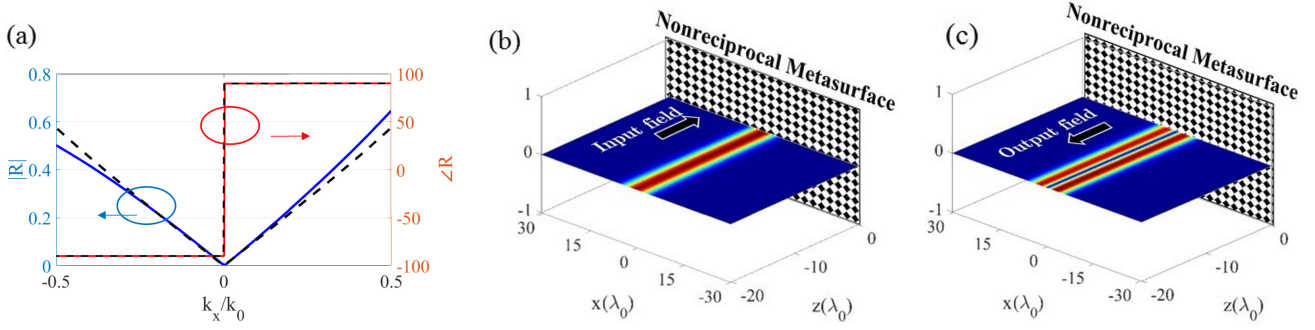


Fig. 2. (a) The synthesized (dashed line) and exact (solid line) transfer functions obtained by a nonreciprocal anisotropic metasurface differentiator characterized with the following polarizabilities: $\alpha_{ee}^{xx} = 1 \times 10^{-20}$, $\alpha_{ee}^{xz} = 2.73 \times 10^{-17}$, $\alpha_{ee}^{zx} = 2.19 \times 10^{-17}$, $\alpha_{ee}^{zz} = 1.21 \times 10^{-18}$, and $\alpha_{mm}^{yy} = 1 \times 10^{-16}$. All quantities are in m^3 . (b) The Gaussian-shape incident field as well as (c) the derivative reflected field along the boresight direction.

$s_{out}(x) = F^{-1} \{s_{inc}(k_x) \tilde{R}(k_x)\}$. The metasurface can be theoretically treated as a bianisotropic homogeneous sheet in its general form with four distinct sets of collective polarizabilities $(\bar{\alpha}_{ee}, \bar{\alpha}_{em}, \bar{\alpha}_{me}, \bar{\alpha}_{mm})$ [35]. Keeping the tensorial format of polarizability components in mind, the reflection coefficient (the transfer function) exerted by the metasurface boundary would be different for s- and p-polarized signals, and we write

$$\bar{H}(k_x) \equiv \begin{bmatrix} \tilde{R}^{s \rightarrow s}(k_x) & \tilde{R}^{s \rightarrow p}(k_x) \\ \tilde{R}^{p \rightarrow s}(k_x) & \tilde{R}^{p \rightarrow p}(k_x) \end{bmatrix} \quad (1)$$

where \tilde{R} alludes to the nonlocal reflection coefficient of the bianisotropic metasurface in the wavevector domain. The first and second superscripts refer to the polarization state of the input and output fields, respectively. Indeed, for an arbitrary input signal having a specific polarization state, the bianisotropic metasurface may suggest two possible transfer functions resulting in two different output signals with s or p polarization in the reflection mode. Each tensorial component of the transfer function in Eq. 1 is affiliated to a certain combination of surface polarizabilities, in an explicit or implicit manner. To unveil these dependencies, we need constitutive parameters which do not change with different conditions of the external excitation and only depend on the physical parameters of the metasurface i.e., the shapes and sizes of the meta-atoms.

With the advent of metasurfaces, a new generation of 2D computational interfaces has emerged to spatially shape the optical fields over deeply sub-wavelength volumes [36]–[38]. Several characterization frameworks based on local tensorial scattering coefficients [39]–[46], surface impedance formulation [47], [48], generalized sheet transition conditions (GSTCs) by susceptibility tensors [49], [50] as well as individual/effective polarizabilities [35], [51]–[53], have been fostered to represent metasurfaces in their general bianisotropic forms. These methods do consider normal components; however, in most studies the normal components are omitted. However, normal components are pivotal when complex spatially-dispersive behavior are demanded in reflection or transmission mode [34]. We thus take these components fully into account and follow the so-called Tretyakov-Simovski formalism relating the fields and polarizations in the general form [35], [52]

$$\mathbf{p} = \bar{\alpha}_{ee} \cdot \mathbf{E}_{inc} + \bar{\alpha}_{em} \cdot \mathbf{H}_{inc} \quad (2)$$

$$\mathbf{m} = \bar{\alpha}_{me} \cdot \mathbf{E}_{inc} + \bar{\alpha}_{mm} \cdot \mathbf{H}_{inc} \quad (3)$$

in which, $\bar{\alpha}_{ee}$, $\bar{\alpha}_{em}$, $\bar{\alpha}_{me}$, and $\bar{\alpha}_{mm}$ are called collective surface polarizabilities: electric, magnetoelectric, electromagnetic, and magnetic ones, respectively. \mathbf{P} and \mathbf{M} also represent the electric and magnetic polarization densities induced on the metasurface. The transversal components of the reflected and transmitted electric fields can be expressed by [52]:

$$\mathbf{E}_{ref,t} = - \left(\bar{I}_t + \bar{Z}_{to} \bar{Y}_{bo} \right)^{-1} \left(\bar{I}_t - \bar{Z}_{to} \bar{Y}_{bo} \right) \cdot \mathbf{E}_{inc,t} - \left(\bar{I}_t + \bar{Z}_{to} \bar{Y}_{bo} \right)^{-1} \cdot \left[j\omega \left(\bar{Z}_{to} \cdot \mathbf{P}_t \pm \mathbf{n} \times \mathbf{M}_t \right) \pm j \left(\mathbf{k}_t \frac{P_n}{\epsilon} \mp \bar{Z}_{to} \cdot (\mathbf{k}_t \times \mathbf{n}) \frac{M_n}{\mu} \right) \right] \quad (4)$$

$$\mathbf{E}_{tran,t} = \left(\bar{I}_t + \bar{Z}_{to} \bar{Y}_{bo} \right)^{-1} \left(\bar{I}_t + \bar{Z}_{to} \bar{Y}_{bo} \right) \cdot \mathbf{E}_{inc,t} - \left(\bar{I}_t + \bar{Z}_{to} \bar{Y}_{bo} \right)^{-1} \cdot \left[j\omega \left(\bar{Z}_{to} \cdot \mathbf{P}_t \mp \mathbf{n} \times \mathbf{M}_t \right) \mp j \left(\mathbf{k}_t \frac{P_n}{\epsilon} \pm \bar{Z}_{to} \cdot (\mathbf{k}_t \times \mathbf{n}) \frac{M_n}{\mu} \right) \right] \quad (5)$$

Here, $\mathbf{P} = \mathbf{p}/S$ and $\mathbf{M} = \mathbf{m}/S$ are polarization surface densities wherein S denotes the unit cell area. Also, the top/bottom sign corresponds to the wave propagating along $\mp z$ direction, and

to and bo in the subscripts refer to top/bottom medium. For the sake of simplicity, we assume the metasurface is surrounded by free-space. Thus, \bar{Z} and $\bar{Y} = \bar{Z}^{-1}$ denoting respectively

the dyadic impedance and admittance of the corresponding medium, can be written as [54]

$$\overline{\overline{Z}} = \eta \begin{bmatrix} \cos \theta \cos^2 \phi + \sin^2 \phi / \cos \theta & (\cos \theta - 1 / \cos \theta) \sin \phi \cos \phi \\ (\cos \theta - 1 / \cos \theta) \sin \phi \cos \phi & \cos \theta \sin^2 \phi + \cos^2 \phi / \cos \theta \end{bmatrix} \quad (6)$$

in which, η is the free-space impedance and θ and ϕ are the elevation and azimuth angles of the incident wave. The formulations above may be applied for any special case of external illumination; for example, s- or p- polarized incident waves or a superposition of these two. To exploit the full potential of the metasurface boundary, each polarizability tensor of Eqs. (2), (3) includes both normal and tangential components, i.e.,

36 scalar polarizabilities which can be written as

$$\overline{\overline{\alpha}}_{ee} = \begin{bmatrix} \alpha_{ee}^{xx} & \alpha_{ee}^{xy} & \alpha_{ee}^{xz} \\ \alpha_{ee}^{yx} & \alpha_{ee}^{yy} & \alpha_{ee}^{yz} \\ \alpha_{ee}^{zx} & \alpha_{ee}^{zy} & \alpha_{ee}^{zz} \end{bmatrix}, \overline{\overline{\alpha}}_{em} = \begin{bmatrix} \alpha_{em}^{xx} & \alpha_{em}^{xy} & \alpha_{em}^{xz} \\ \alpha_{em}^{yx} & \alpha_{em}^{yy} & \alpha_{em}^{yz} \\ \alpha_{em}^{zx} & \alpha_{em}^{zy} & \alpha_{em}^{zz} \end{bmatrix} \quad (7)$$

$$\overline{\overline{\alpha}}_{me} = \begin{bmatrix} \alpha_{me}^{xx} & \alpha_{me}^{xy} & \alpha_{me}^{xz} \\ \alpha_{me}^{yx} & \alpha_{me}^{yy} & \alpha_{me}^{yz} \\ \alpha_{me}^{zx} & \alpha_{me}^{zy} & \alpha_{me}^{zz} \end{bmatrix}, \overline{\overline{\alpha}}_{mm} = \begin{bmatrix} \alpha_{mm}^{xx} & \alpha_{mm}^{xy} & \alpha_{mm}^{xz} \\ \alpha_{mm}^{yx} & \alpha_{mm}^{yy} & \alpha_{mm}^{yz} \\ \alpha_{mm}^{zx} & \alpha_{mm}^{zy} & \alpha_{mm}^{zz} \end{bmatrix} \quad (8)$$

With substituting Eqs. 2, 3, 7, 8 into Eqs. 4, 5 and after some algebraic manipulations, the most general form for the co-polarized reflection and transmission coefficients of the metasurface can be obtained as:

$$R_{\pm}^{s \rightarrow s} = \frac{-j\omega}{2} \left[\frac{\eta}{\cos \theta} \alpha_{ee}^{yy} \pm \alpha_{em}^{yx} \mp \tan \theta \alpha_{em}^{yz} \mp \alpha_{me}^{xy} - \frac{\cos \theta}{\eta} \alpha_{mm}^{xx} + \frac{\sin \theta}{\eta} \alpha_{mm}^{xz} \mp \tan \theta \alpha_{me}^{zy} - \frac{\sin \theta}{\eta} \alpha_{mm}^{zx} + \frac{\sin \theta \tan \theta}{\eta} \alpha_{mm}^{zz} \right] \quad (9)$$

$$T_{\pm}^{s \rightarrow s} = 1 - \frac{j\omega}{2} \left[\frac{\eta}{\cos \theta} \alpha_{ee}^{yy} \pm \alpha_{em}^{yx} \mp \tan \theta \alpha_{em}^{yz} \pm \alpha_{me}^{xy} + \frac{\cos \theta}{\eta} \alpha_{mm}^{xx} - \frac{\sin \theta}{\eta} \alpha_{mm}^{xz} \mp \tan \theta \alpha_{me}^{zy} - \frac{\sin \theta}{\eta} \alpha_{mm}^{zx} + \frac{\sin \theta \tan \theta}{\eta} \alpha_{mm}^{zz} \right] \quad (10)$$

$$R_{\pm}^{p \rightarrow p} = \frac{-j\omega}{2} \left[\eta \cos \theta \alpha_{ee}^{xx} \mp \alpha_{em}^{xy} - \eta \sin \theta \alpha_{ee}^{xz} \pm \alpha_{me}^{yx} - \frac{1}{\eta \cos \theta} \alpha_{mm}^{yy} \mp \tan \theta \alpha_{me}^{yz} + \eta \sin \theta \alpha_{ee}^{zx} \mp \tan \theta \alpha_{em}^{zy} - \eta \sin \theta \tan \theta \alpha_{ee}^{zz} \right] \quad (11)$$

$$T_{\pm}^{p \rightarrow p} = 1 - \frac{j\omega}{2} \left[\eta \cos \theta \alpha_{ee}^{xx} \mp \alpha_{em}^{xy} - \eta \sin \theta \alpha_{ee}^{xz} \mp \alpha_{me}^{yx} + \frac{1}{\eta \cos \theta} \alpha_{mm}^{yy} \pm \tan \theta \alpha_{me}^{yz} - \eta \sin \theta \alpha_{ee}^{zx} \pm \tan \theta \alpha_{em}^{zy} + \eta \sin \theta \tan \theta \alpha_{ee}^{zz} \right] \quad (12)$$

These equations reveal the angular dispersion behavior of the reflection and transmission coefficients for a non-reciprocal bianisotropic metasurface in its general form with 36 tensorial components and will be instrumental for the discussions presented in the following sections.

B. Nonreciprocal on-axis differentiator

The main goal of this paper is to search for the best group of polarizability components whereby the reflection or transmission coefficient in Eqs. (9)-(12), $\mathbf{R}(\mathbf{k}_x)$ or $\mathbf{T}(\mathbf{k}_x)$, obeys the angular dispersion of the desired mathematical operator. The first-order differentiation operation is a good representative for the family of asymmetric OTFs. Referring to $\hat{H}(\mathbf{k}_x) = j\mathbf{k}_x$ for the first-order differentiation operator, our purpose is to realize an on-axis reflective channel whose transfer function, $\hat{R}(\mathbf{k}_x)$, has indispensably a non-local odd-symmetric treatment around $\theta = 0$ without polarization rotation, i.e., $R(\theta) = R(-\theta)$. Let us consider the conceptual illustration of Fig. 1b in which the possibility of $R(\theta) \neq R(-\theta)$ is graphically investigated. A first-order, polarization-preserving, differentiation operation requires that the co-polarized reflection coefficient imparted on the plane wave coming from $R_{2 \rightarrow 1}$ channel (θ illumination) essentially differs from that seen from $R_{1 \rightarrow 2}$ channel ($-\theta$ illumination), which is prohibited by reciprocity. So, resorting to a non-reciprocal metasurface is inevitable to implement

a polarization-preserved first-order differentiator for on-axis illuminations [29]. This observation can be verified through Eqs. (9), (11) in which the necessary condition to keep terms with odd functionality from θ is $\alpha_{em}^{yz} \neq -\alpha_{me}^{zy}$ or $\alpha_{mm}^{xz} \neq \alpha_{mm}^{zx}$ for s-polarized incidences and $\alpha_{ee}^{xz} \neq \alpha_{ee}^{zx}$ or $\alpha_{me}^{yz} \neq -\alpha_{em}^{zy}$ for p-polarized incidences. These constraints for polarization-preserved reflective optical processing obviously break the Casimir-Onsager reciprocity relations [55]. However, as can be directly inferred from Eqs. (10), (12), polarization-preserving on-axis asymmetric OTFs in transmission regime can be simply implemented by using a reciprocal metasurface having non-zero α_{mm}^{xz} and α_{ee}^{xz} for s- and p-polarized incidences, respectively.

As a representative example, let us consider the following synthesis problem: find the surface polarizabilities of a nonreciprocal metasurface for which a p-polarized input field with an illumination angle of $\theta_{inc} = 0^\circ$ reflects into a co-polarized beam whose profile is the first-order derivative of the one of the input. A Gaussian-shape beam profile with a spatial bandwidth of $W = 0.2k_0$ is considered as the input field. In order to obtain the required surface polarizabilities, the metasurface synthesis will be treated as a non-linear optimization problem which is solved numerically. Firstly, according to the scattering role of each polarizability component, the neutral components are assumed to be zero. The involved polarizabilities are α_{ee}^{xx} , α_{ee}^{xz} , and α_{ee}^{zx} , α_{ee}^{zz} , and α_{mm}^{yy} .

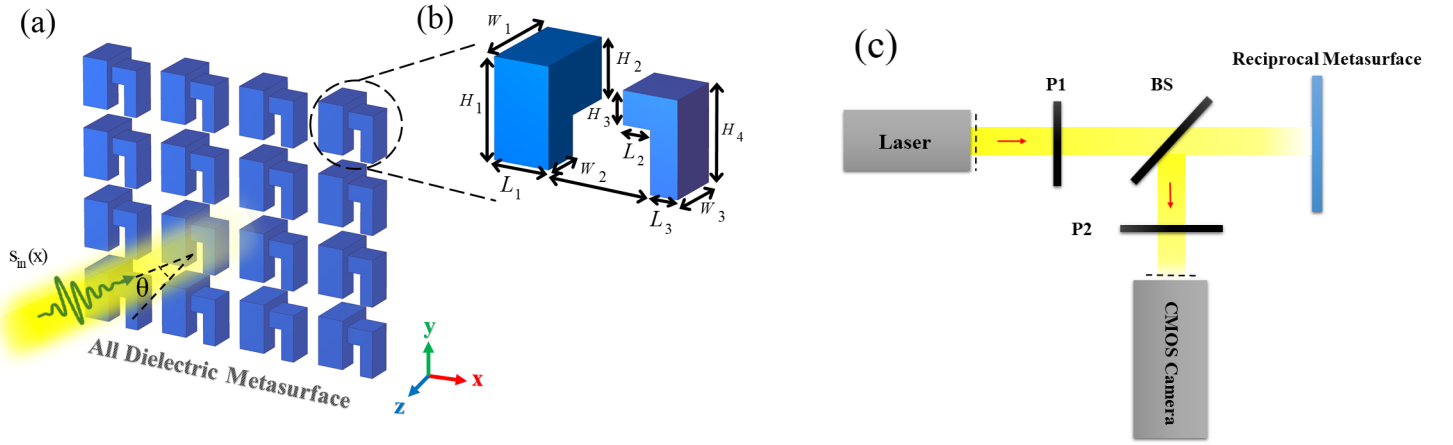


Fig. 3. (a) The array of polarizable meta-atoms for performing optical signal processing. (b) The proposed reciprocal bianisotropic meta-atom exposing normal polarizability components. The geometry was chosen in such a way that both symmetries in xy - and yz - planes are broken. The geometrical parameters are $L_1=410$ nm, $L_2=205$ nm, $L_3=205$ nm, $L_4=350$ nm, $w_1=695$ nm, $w_2=315$ nm, $w_3=410$ nm, $H_1=760$ nm, $H_2=455$ nm, $H_3=250$ nm, and $H_4=730$ nm. (c) The schematic setup for testing the optical signal processing performance of the reflective metasurface in which P and BS stand for the polarizer and beam splitter, respectively.

Then, we seek for those surface polarizabilities for which the difference between the desired GF, $\tilde{G}_{\text{des}}(k_x)=jk_x$, and the angle-dependent reflection coefficient of the metasurface, $\tilde{R}(k_x)$, is minimized within a pre-determined angular range. The cost function is defined as the sum of squares of the differences at a finite number of N samples for both real and imaginary parts $f = w_{\text{re}} \sum_{i=1}^N \left(\text{Re} \left[\tilde{G}_{\text{des}}(k_{x,i}) - \tilde{R}(k_{x,i}) \right] \right)^2 + w_{\text{im}} \sum_{i=1}^N \left(\text{Im} \left[\tilde{G}_{\text{des}}(k_{x,i}) - \tilde{R}(k_{x,i}) \right] \right)^2$. Here, w_{re} and w_{im} represent the weight coefficients established to selectively adjust the contribution of real and imaginary parts, respectively. At this stage, the metasurface processor is synthesized with the optimized polarizabilities shown in the caption of Fig. 2. It should be noted that, since $\alpha_{\text{ee}}^{\text{xz}}$ is not equal to $\alpha_{\text{ee}}^{\text{zx}}$, the synthesized metasurface is non-reciprocal. The resultant transfer functions along with the input and output fields are displayed in Figs. 2a-c. These figures show good agreement between the desired and synthesized transfer functions and output beam profiles. Indeed, the reflected field propagating out along the boresight direction is the 1st-order derivative of the Gaussian-shape input field. The accuracy of differentiation is 99.5%, described by the Pearson correlation coefficient between the simulated and exact reflected field amplitudes. The results confirm that at the expense of a complex fabrication, a suitably

designed nonreciprocal anisotropic metasurface can be thought of as a reflective optical 1st-order differentiator working for input fields coming from normal direction.

C. Reciprocal on-axis differentiator

As an alternative solution, incorporating cross-polarization channels to the problem can elaborately circumvent the nettle restrictions arising from reciprocity. In this case, the polarizability components are engineered so that the polarization state of the incident light coming from Port 1 be rotated when it is captured at Port 2 (see Fig. 1b). Hereafter, the cross-polarized reflection of $R^{s \rightarrow p}$ or $R^{p \rightarrow s}$ serves as the transfer function of our processing channel meaning that the output signal has orthogonal polarization with respect to that of the input wave. It should be noted that such a metasurface, if designed, will exhibit $R_{1 \rightarrow 2}^{s \rightarrow p} \neq R_{2 \rightarrow 1}^{s \rightarrow p}$ which no longer quashes the reciprocity condition. Similar deduction can be made for $R_{1 \rightarrow 2}^{p \rightarrow s} \neq R_{2 \rightarrow 1}^{p \rightarrow s}$. Due to the insensitivity of conventional optical sensors, including the human eyes, to the polarization of light, polarization rotation does not degrade the overall performance of optical differentiator, instead, it dramatically facilitates the realization procedure. Based on Eqs. (2)-(8), the cross-polarized reflection and transmission coefficients of the metasurface read as:

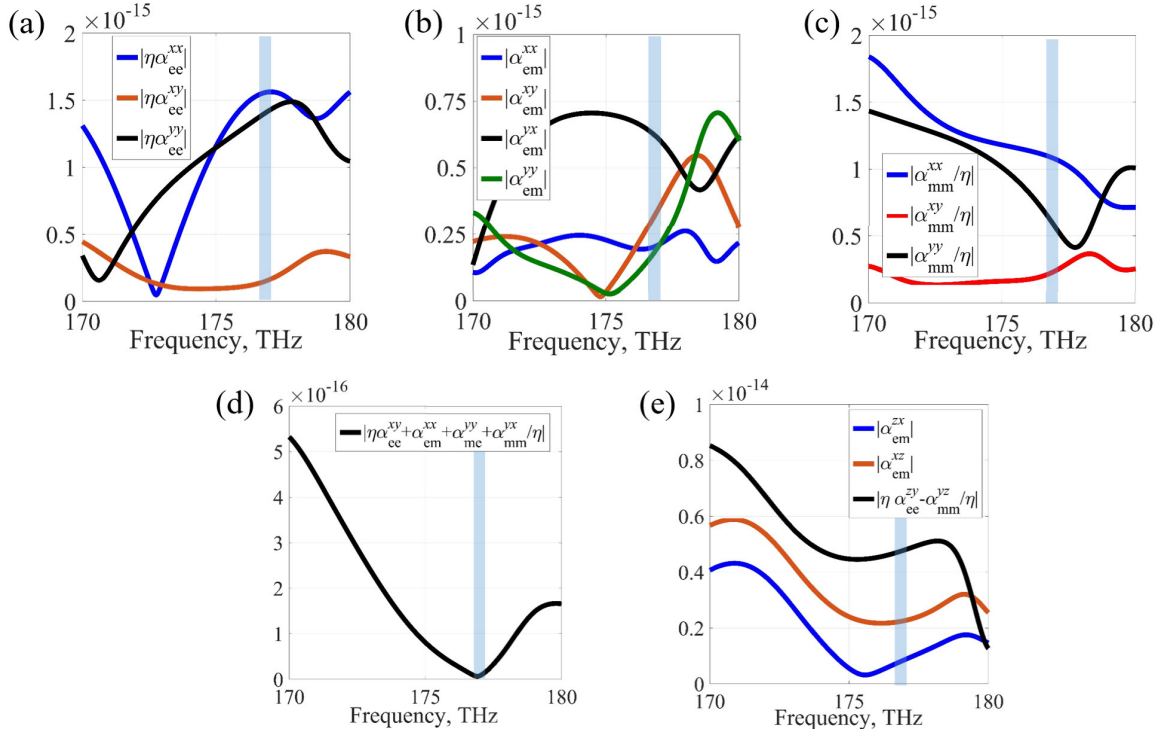


Fig. 4. (a), (b), (c) The tangential collective polarizabilities of the designed optical metasurface given in Fig. 3a. Evaluation of (d) zero cross-polarized reflection and (e) asymmetric angular dispersion conditions on the surface polarizabilities. The working frequency is $f=177$ THz and is highlighted by a blue marker in the figures.

$$R^{s \rightarrow p} = \frac{-j\omega}{2} \left[\eta\alpha_{ee}^{xy} \pm \cos\theta\alpha_{em}^{xx} \mp \sin\theta\alpha_{em}^{xz} \pm \frac{\alpha_{me}^{yy}}{\cos\theta} + \frac{1}{\eta}\alpha_{mm}^{yx} - \frac{\tan\theta}{\eta}\alpha_{mm}^{yz} + \eta\tan\theta\alpha_{ee}^{zy} \pm \sin\theta\alpha_{em}^{zx} \mp \sin\theta\tan\theta\alpha_{em}^{zz} \right] \quad (13)$$

$$T^{s \rightarrow p} = -\frac{j\omega}{2} \left[\eta\alpha_{ee}^{xy} \pm \cos\theta\alpha_{em}^{xx} \mp \sin\theta\alpha_{em}^{xz} \mp \frac{\alpha_{me}^{yy}}{\cos\theta} - \frac{1}{\eta}\alpha_{mm}^{yx} + \frac{\tan\theta}{\eta}\alpha_{mm}^{yz} - \eta\tan\theta\alpha_{ee}^{zy} \mp \sin\theta\alpha_{em}^{zx} \pm \sin\theta\tan\theta\alpha_{em}^{zz} \right] \quad (14)$$

$$R^{p \rightarrow s} = \frac{-j\omega}{2} \left[\eta\alpha_{ee}^{yx} \mp \frac{1}{\cos\theta}\alpha_{em}^{yy} - \eta\tan\theta\alpha_{ee}^{yz} \mp \cos\theta\alpha_{me}^{xx} + \frac{1}{\eta}\alpha_{mm}^{xy} \pm \sin\theta\alpha_{me}^{xz} \mp \sin\theta\alpha_{me}^{zx} + \frac{\tan\theta}{\eta}\alpha_{mm}^{zy} \pm \sin\theta\tan\theta\alpha_{me}^{zz} \right] \quad (15)$$

$$T^{p \rightarrow s} = -\frac{j\omega}{2} \left[\eta\alpha_{ee}^{yx} \mp \frac{1}{\cos\theta}\alpha_{em}^{yy} - \eta\tan\theta\alpha_{ee}^{yz} \pm \cos\theta\alpha_{me}^{xx} - \frac{1}{\eta}\alpha_{mm}^{xy} \mp \sin\theta\alpha_{me}^{xz} \mp \sin\theta\alpha_{me}^{zx} + \frac{\tan\theta}{\eta}\alpha_{mm}^{zy} \pm \sin\theta\tan\theta\alpha_{me}^{zz} \right] \quad (16)$$

It should be remembered that we are seeking for those reciprocal collective polarizability tensors which can be potentially effective to satisfy two important conditions at the same time: exciting the cross-polarization reflected fields and making the cross-polarized reflection to be an asymmetric function of k_x (or θ) variable. As clearly seen from Eqs. (13), (15), although the presence of 9 surface polarizabilities leads to generation of cross-polarized reflection fields for each of s- and p-polarized illuminations, only 4 of them deal with odd-order terms (with respect to θ). Indeed, the necessary condition for reciprocal realization of on-axis asymmetric OTFs in the cross-polarized reflective channel is the presence of

rule I:

$$\alpha_{em}^{xz} \text{ or } \alpha_{mm}^{yz} \text{ or } \alpha_{ee}^{zy} \text{ or } \alpha_{em}^{zx} \text{ (s-polarized illumination)}$$

$$\alpha_{ee}^{yz} \text{ or } \alpha_{me}^{xz} \text{ or } \alpha_{me}^{zx} \text{ or } \alpha_{mm}^{zy} \text{ (p-polarized illumination)}$$

This means that the role of normal polarizabilities and bianisotropy is undeniable for a reciprocal metasurface to build asymmetric angular dispersion behavior for the reflection around $k_x=0$. We call these surface polarizability components Cross-polarization Exciting Normal Polarizabilities (CPENP) throughout the paper. The cross-polarized transmission processing channel can also be enabled if the surface polarizabilities α_{mm}^{yz} or α_{ee}^{zy} for s-polarized illumination and α_{ee}^{yz} or α_{mm}^{zy} for p-polarized input signals contribute to the overall scattering of the metasurface. For the specular case of first-order differentiation operator, $R^{cr}(k_x=0)=0$ meaning that no cross-polarized field should exist upon illuminating

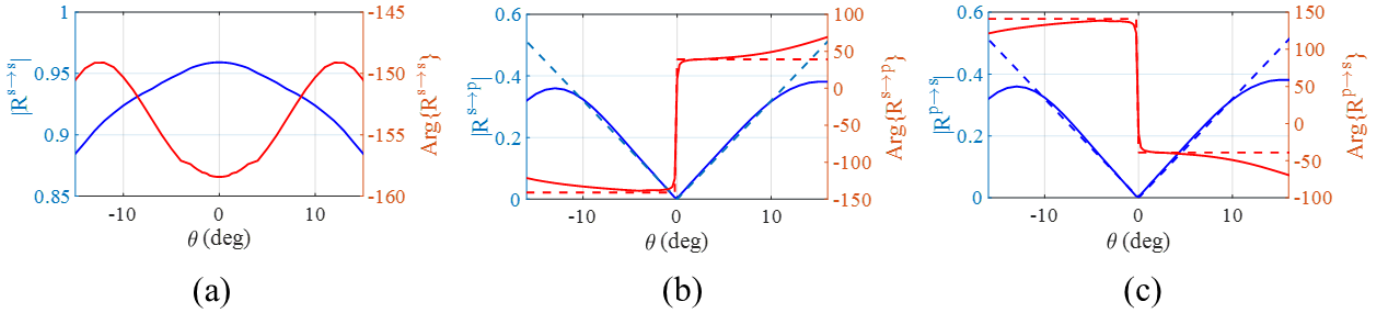


Fig. 5. The phase and amplitude of (a) co-polarized and (b), $s \rightarrow p$ and (c) $p \rightarrow s$ reflection coefficients. The phase and amplitude of the exact transfer function for implementing the first-order differentiation operation are also presented. The solid- and dashed-lines stand for the exact and the synthesized transfer functions, respectively, and the working frequency is $f=177$ THz.

by on-axis plane waves. Mathematically speaking, Eqs. (13), (15) implies that

rule II:

$$\eta \alpha_{ee}^{xy} \pm \alpha_{em}^{xx} \pm \alpha_{me}^{yy} + \frac{1}{\eta} \alpha_{mm}^{yx} = 0 \text{ (s-polarized illumination)}$$

$$\eta \alpha_{ee}^{yx} \mp \alpha_{em}^{yy} \mp \alpha_{me}^{xx} + \frac{1}{\eta} \alpha_{mm}^{xy} = 0 \text{ (p-polarized illumination)}$$

must be satisfied, because otherwise, the metasurface may expose non-zero cross-polarized reflection at $\theta=0$. In summary, among all possible types of bianisotropy and longitudinal polarizabilities, specific solutions are desired which have been comprehensively discussed above. As an important deduction from Fig. 1b, the reciprocity enforces $R^{s \rightarrow p}(\theta) = R^{p \rightarrow s}(-\theta)$ meaning that the mirror version of each mathematical operator realized by $R^{s \rightarrow p}$ channel, $\tilde{H}(\mathbf{k}_x)$, will also be constructed by $R^{p \rightarrow s}$ channel, $\tilde{H}(-\mathbf{k}_x)$. Indeed, the proposed approach is inherently dual-polarized and can be applied to both s - and p -polarized input signals for many types of transfer functions like spatial differentiation and integration for which $\tilde{H}(-\mathbf{k}_x)$ still yields a usable output wave. This interesting feature which has been rarely reported in the literature may find great potential applications in dual-polarized optical computations [17], [31].

III. DUAL-POLARIZED OPTICAL SIGNAL AND IMAGE PROCESSING

As known, the macroscopic scattering features of any metasurface is mainly determined by properties of its constituent meta-atoms in the microscopic scale [50], [52]. In this section, we demonstrate that the proposed all-dielectric optical metasurface shown in Fig. 3a exposes the same collective polarizabilities required for performing first-order spatial differentiation at the macroscopic view. The meta-atom of Fig. 3a comprises two non-identical L-shaped dielectric particles with a relative 90-degree rotation. The meta-atoms are made of silicon (Si) material whose relative permittivity is extracted

from Palik's book [56]. A comprehensive parametric study has been accomplished to search for the best group of parameters making the angular dispersion of the cross-polarized reflection coefficient of the dielectric particles as close to the desired transfer function as possible. The dielectric inclusions are periodically repeated with the periodicity of $1.1 \mu\text{m}$ and $0.9 \mu\text{m}$ along the both x and y directions, respectively. The angular dependency of the scattering properties reflect the symmetry of the meta-atoms. There are three possible types of symmetries [34]: 180° -rotation symmetry around the y -axis (C_2), reflection symmetry through the x -axis (σ_x) and reflection symmetry through the z -axis (σ_z). If the scattering particles do not exhibit any structural symmetry, then the resulting metasurface corresponds to a bianisotropic structure with both normal and tangential polarization densities and its angular scattering response does not present any symmetry in addition to those imposed by reciprocity [34], [51]. As a consequence, as we can see in Fig. 3b, we break the mentioned geometrical symmetries in order to obtain a reciprocal bianisotropic metasurface whose CPENP are effectively excited at oblique incidences. Based on the retrieval procedure presented in [51], [57], the in-plane collective polarizabilities of the designed metasurface have been extracted. In fact, after the dipole approximation of meta-atoms in a polarizability retrieval setup, the metasurface is illuminated by four normally incident plane waves, and the tangential polarizations can be described in terms of induced dipole moments. By applying an equivalent surface model for the bianisotropic sheet, the *tangential* collective polarizabilities can be calculated as a function of the reflection/transmission coefficients from the array. The retrieved results are displayed in Figs. 4a-c. Moreover, the zero cross-polarized reflection condition of the surface polarizabilities at the normal incidence has been assessed in Fig. 4d. As seen, the rule II is satisfied in the vicinity of 177 THz at which the metasurface creates no on-axis cross-polarized fields at the reflection side. Hereafter, we intend to distinguish which one of the CPENP is provided by the designed metasurface. After some mathematical manipulations on Eqs. (13), (15) and with applying the reciprocity constraints, we have:

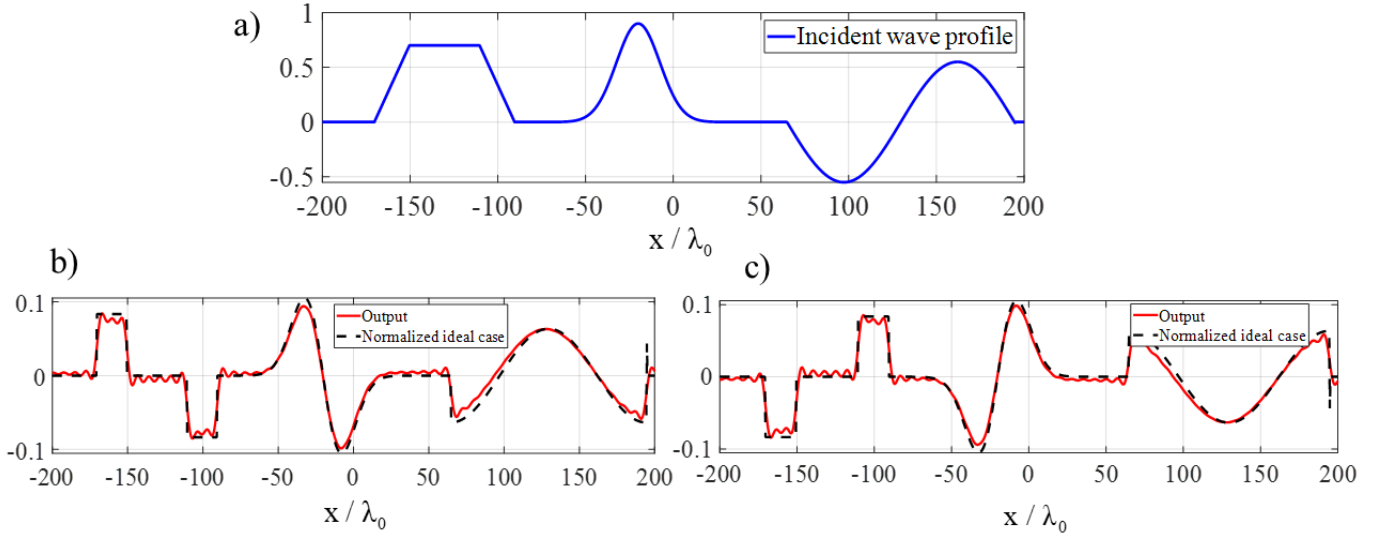


Fig. 6. (a) Field profile of the input signal, formed by a combination of trapezoidal, Gaussian, and sinusoidal functions (b), (c) the $s \to p$ and $p \to s$ reflected field profiles, respectively. The exact derivative signals have been also presented for the sake of comparison. The metasurface is illuminated from normal direction and the working frequency is $f=177$ THz.

$$\alpha_{em}^{xz} = -\alpha_{me}^{zx} = \frac{1}{j2\omega \sin \theta} \left[\left(R_{\theta,+}^{s \to p} - R_{-\theta,+}^{s \to p} \right) + \left(T_{\theta,+}^{s \to p} - T_{-\theta,+}^{s \to p} \right) \right] \quad (17)$$

$$\alpha_{em}^{zx} = -\alpha_{me}^{xz} = \frac{1}{-j2\omega \sin \theta} \left[\left(R_{\theta,+}^{s \to p} - R_{-\theta,+}^{s \to p} \right) + \left(T_{\theta,-}^{s \to p} - T_{-\theta,-}^{s \to p} \right) \right] \quad (18)$$

$$\eta \alpha_{ee}^{zy} - \frac{1}{\eta} \alpha_{mm}^{yz} = \frac{1}{-j2\omega \tan \theta} \left[\left(R_{\theta,+}^{s \to p} - R_{\theta,-}^{s \to p} \right) - \left(T_{\theta,+}^{s \to p} - T_{\theta,-}^{s \to p} \right) \right] \quad (19)$$

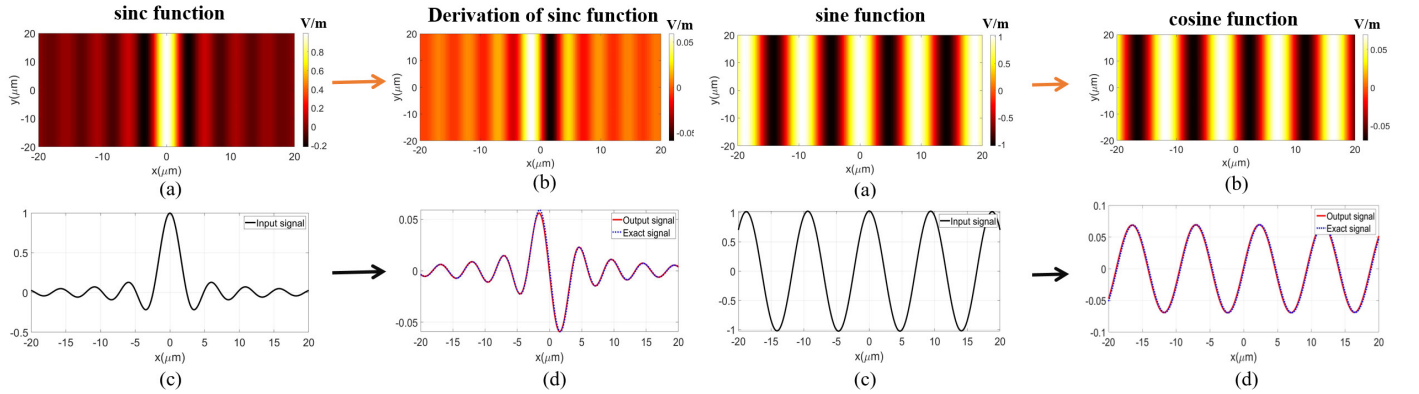


Fig. 7. (a), (c) The s -polarized sinc-shape incident field profile together with (b), (d) the p -polarized reflected derivative field profile. The exact derivative signals have been also presented for the sake of comparison. The reciprocal metasurface is illuminated from normal direction and the working frequency is $f=177$ THz.

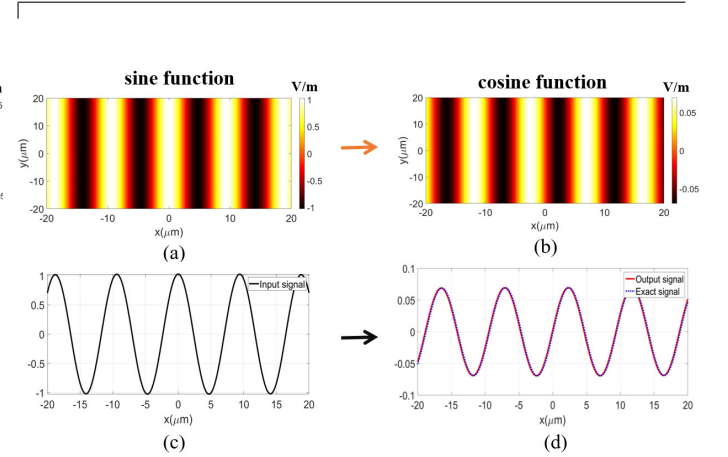


Fig. 8. (a), (c) The p -polarized sinc-shape incident field profile together with (b), (d) the s -polarized reflected derivative field profile. The exact derivative signals have been also presented for the sake of comparison. The reciprocal metasurface is illuminated from normal direction and the working frequency is $f=177$ THz.

Four s -polarized oblique plane waves illuminating the metasurface along forward and backward directions serve to extract some information regarding the normal components of the collective polarizabilities. By using an arbitrary small incident wave angle $\theta=4^\circ$, all required scattering parameters in Eqs. (17)-(19) have been simulated and the left-hand side parameters are plotted in Fig. 4e. As can be seen, the results clearly

demonstrate that around 177 THz, among eight possible CPENP, the impact of $\eta \alpha_{ee}^{zy} - \frac{1}{\eta} \alpha_{mm}^{yz}$ is more tangible while the role of α_{em}^{zx} can be neglected. Indeed, the engineered geometry of the designed reciprocal meta-atom makes it as a suitable choice for realizing on-axis asymmetric OTFs in the reflection side.

For instance, the cross-polarized reflection coefficient of

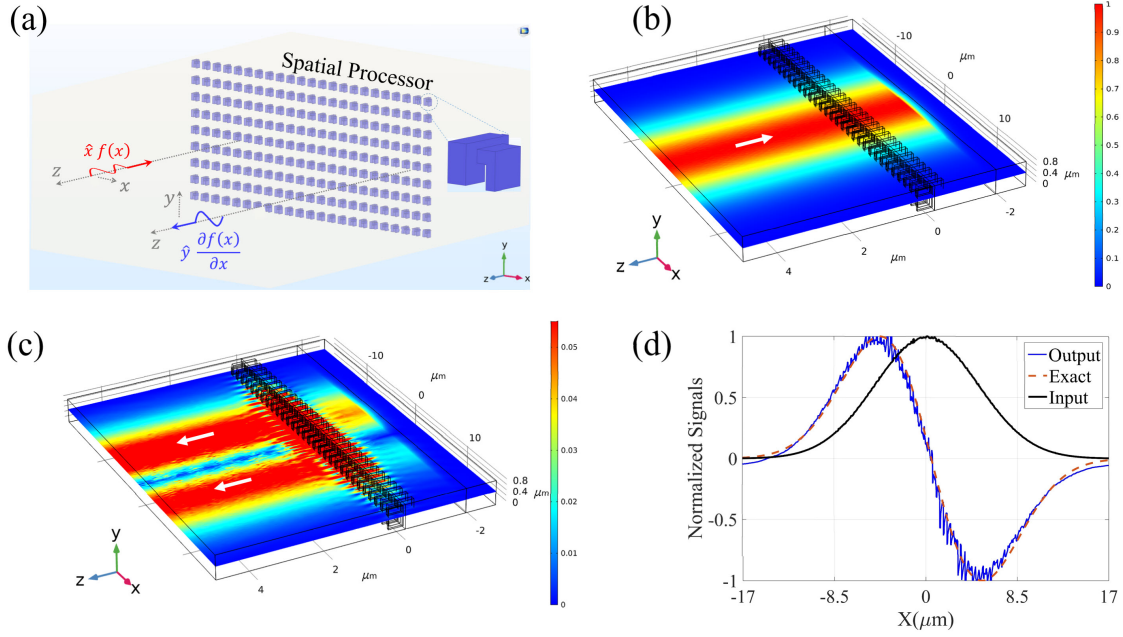


Fig. 9. The 3D full-wave simulation for verification of the proposed on-axis differentiation method. (a) The finite array of all-dielectric meta-atoms, (b) the intensity of the x-polarized incident field (input signal), (c) the intensity of the y-polarized reflected field (output signal), (d) a comparison between the cross-polarized reflected field and the exact derivative of the input signal at the distance $5\lambda_0$ from the bianisotropic metasurface.

the array can be tailored to mimic the angular trend of $R^{s \rightarrow p}(\theta) = j\zeta \sin(\theta)$. The parameter ζ stands for the gain of differentiator which depends on the value of surface polarizabilities. Through engineering the meta-atom geometry, one can achieve a cross-polarized response that approximates the nonlocal behavior of the first-derivative operation with a phase jump at $k_x=0$. The phase and amplitude of the co- and cross-polarized reflection coefficients at $f=177$ THz are plotted in Figs. 5a-c, respectively. The results are numerically recorded by using CST full-wave commercial software, where periodic boundary conditions are applied to the x- and y-directed walls and Floquet ports are considered along the z direction. The first deduction is that the co-polarized reflection coefficient possesses a symmetric response with respect to k_x due to the reciprocity theorem (Fig. 5a). The second inference is that, as expected from the presented analysis, the cross-polarized reflection for both s- and p-polarized incidences, possesses an odd-symmetric spatial trend around $k_x=0$. Owing to the reciprocity constraint and $\tilde{R}^{s \rightarrow p}(k_x) = -\tilde{R}^{s \rightarrow p}(-k_x)$, the results of Figs. 5b, c differ only in the phase sign. The exact amplitude and phase of the transfer function representing the first-order differentiation operation are fairly compared with those synthesized by the designed metasurface. An excellent agreement between the cross-polarization reflection of the designed metasurface and the exact transfer function has been achieved as long as the normalized spatial bandwidth of the input signals lies within $|k_x/k_0| < 0.25$. This range essentially provides the maximum spatial resolution of input signals that can be correctly processed by the designed optical metasurface. It should be noted that the effects of losses are included in the numerical results. They are modeled by a non-zero imaginary part in the dielectric constant of silicon. Moreover, due to the intrinsic $\chi^{(3)}$ nonlinear behavior of

silicon, the optical response of the designed meta-atom slightly changes in the case of extremely high optical intensities. In fact, the first order correction due to the nonlinear Kerr effect is a dependency of the refractive index to the optical intensity, i.e., $\varepsilon = \varepsilon_{lin} + \chi^{(3)}|E|^2$, and $\chi^{(3)} = 2.8 \times 10^{-18} \text{ m}^2/\text{V}^2$ [58]. Since $\chi^{(3)}$ is small, the nonlinear effects only appear when the optical intensity is very large. Our simulations confirm that the performance of the signal/image processing predicted by the linear limit is not deteriorated as long as the optical intensity remains below tens of GW/cm^2 . Therefore, optical signal processing can be safely performed without being affected by nonlinear effects, even at moderate intensity levels.

To inspect the differentiation performance of the employed metasurface processor, a complex signal which is a combination of trapezoidal, Gaussian, and sinusoidal functions (see Fig. 6a), has been utilized as the beam profile of the on-axis incidence. The details for the schematic setup are shown in Fig. 3c. The polarizers are utilized to filter out the unwanted polarization in each case and the beam splitter is aimed at directing the reflected fields to the camera. The cross-polarized reflections egressing the metasurface from $s \rightarrow p$ and $p \rightarrow s$ normal processing channels are captured as output signals and the corresponding results are illustrated Figs. 6b, c, respectively. The output signals were in this manner: Each plane wave impinging on the metasurface will be reflected with a certain reflection coefficient corresponding to its incident wave angle, $\tilde{R}(k_x)$. In this case, the angular spectrum of the output fields is given by

$$\tilde{g}_{ch1}(k_x) = \tilde{R}^{s \rightarrow p}(k_x) \tilde{f}_{ch1}(k_x) \quad (20)$$

$$\tilde{g}_{ch2}(k_x) = \tilde{R}^{p \rightarrow s}(k_x) \tilde{f}_{ch2}(k_x) \quad (21)$$

in reflection mode. Here, the subscripts denote the number of processing channel. Thus, the synthesized output fields can be numerically calculated as:

$$E_{\text{ref, ch1}} = \int_{k_{0x}-W}^{k_{0x}+W} \tilde{R}^{s \rightarrow p}(k_x) \tilde{f}_{\text{ch1}}(k_x) \exp(-jk_x x - jk_z z) dk_x \quad (22)$$

$$E_{\text{ref, ch2}} = \int_{k_{0x}-W}^{k_{0x}+W} \tilde{R}^{p \rightarrow s}(k_x) \tilde{f}_{\text{ch2}}(k_x) \exp(-jk_x x - jk_z z) dk_x \quad (23)$$

As can be seen, the all-dielectric optical metasurface successfully implements the first-order differentiation of the input signal at both output terminations. Indeed, when the input signal is reflected by the metasurface, the flat regimes are filtered out, the linear segments are converted to flat ones, the sine is converted to the cosine one, and finally, the descending and ascending parts of the Gaussian signal are distinguished. To evaluate the performance of our metasurface differentiator, the numerically-obtained results are compared with the exact first-derivative of the input signals in the same figures. The results are exactly the responses expected from a first-derivative operation with only 2% error according to $e_f = (\|s_{\text{out}}^{\text{exact}}(x) - s_{\text{out}}^{\text{simul}}(x)\|) / \|s_{\text{out},x}^{\text{ideal}}(x)\|$. Therefore, the effective role of CPENP in constructing odd-symmetric nonlocal reflection suggests a new reciprocal way to realize first-order spatial differentiation for normal illuminations. It should be mentioned that the designed metasurface is suitable for optical applications [35].

The metasurface processor is dual-polarized and the processing channel can also carry a couple of input/output signals, separately. Two distinct 1D signals (sinc and sinusoidal functions) representing the beam-profiles of s- and p-polarized on-axis incidences are considered as the input signals (see Figs. 7a, c and Figs. 8a, c). As can be noticed from Figs. 7b, d and Figs. 8b, d, both orthogonal channels can separately serve to construct the first-order derivative of the corresponding input fields at the output termination.

To further verify the performance of the proposed metasurface differentiator, 3D full-wave simulations have been carried out (COMSOL Multiphysics). An x-polarized Gaussian beam is normally incident on the array of meta-atoms. The medium surrounding the bianisotropic metasurface is filled by air. The boundary conditions are selected as perfectly matched layers (PMLs), and periodic along x and y directions, respectively. Figs. 9a, b demonstrate the intensity of the incident field and of the cross-polarized reflected field, respectively. Moreover, Fig. 9c shows a cut-line of the normalized reflected field at a distance $5 \lambda_0$ from the bianisotropic metasurface. The result of the full-wave simulation is compared with the exact first-order derivative of the input signal. As noticed, an excellent agreement has been obtained. More particularly, the positive and negative slopes of the input signal are clearly revealed in the cross-polarized reflected fields.

IV. CONCLUSION

To conclude, for the first time, we exploited the full macroscopic potential of a reciprocal bianisotropic metasurface to realize dual-polarized asymmetric OTFs at on-axis reflective processing channels. We analytically demonstrated how the cross-polarization channel governed by the CPENP can simply break the angular reflection of the metasurface around $\theta=0$ and mimic the k_x -asymmetric spatially-dispersive transfer functions. Motivated by the existing relation between the angular scattering and geometrical mirror symmetries in the microscopic scale, the realization possibility of the proposed design was assessed through proposing an all-dielectric meta-atom and retrieving its important surface polarizabilities. The numerical simulations illustrated that the proposed metasurface reflects the first-derivative of the input signals, with either s or p polarization, coming from the normal direction, without using any bulky Fourier lens. The analytical design method presented in this paper can be extended to 2D scenarios by involving k_y wavenumber into the relations and obtaining explicit or implicit expression for $\tilde{R}(k_x, k_y)$. Therefore, the designed all-dielectric metasurface offers a simple and ultra-thin normally-oriented channel to perform optical signal/image processes without complicated settings arising from oblique illuminating setups or resorting to nonreciprocal media. Meanwhile, the proposed reflective processing system is more compatible with the current demands on the integrated devices than the transmissive ones while offering a promising vision for realizing parallel computations using both reflection and transmission channels.

Acknowledgements - A.M. and R.F. acknowledge support from the Swiss National Science Foundation (SNSF) under the Eccellenza award number 181232.

REFERENCES

- [1] J. Goodman, "Introduction to fourier optics," 2008.
- [2] H. Stark, *Application of Optical Fourier Transforms*. Elsevier, 2012.
- [3] D. Mendlovic and H. M. Ozaktas, "Fractional fourier transforms and their optical implementation: I," *JOSA A*, vol. 10, no. 9, pp. 1875–1881, 1993.
- [4] J. Nakamura, *Image sensors and signal processing for digital still cameras*. CRC press, 2017.
- [5] A. Bogoni, L. Poti, R. Proietti, G. Meloni, F. Ponzini, and P. Ghelfi, "Regenerative and reconfigurable all-optical logic gates for ultra-fast applications," *Electronics Letters*, vol. 41, no. 7, pp. 435–436, 2005.
- [6] L. Brzozowski and E. H. T. Sargent, "All-optical analog-to-digital converters, hardlimiters, and logic gates," *Journal of lightwave technology*, vol. 19, no. 1, p. 114, 2001.
- [7] J. McGeehan, M. Giltreli, and A. Willner, "All-optical digital 3-input and gate using sum-and difference-frequency generation in p1pn waveguide," *Electronics Letters*, vol. 43, no. 7, pp. 409–410, 2007.
- [8] J. Xu, X. Zhang, J. Dong, D. Liu, and D. Huang, "All-optical differentiator based on cross-gain modulation in semiconductor optical amplifier," *Optics letters*, vol. 32, no. 20, pp. 3029–3031, 2007.
- [9] M. A. Al-Alaoui, "Novel digital integrator and differentiator," *Electronics letters*, vol. 29, no. 4, pp. 376–378, 1993.
- [10] N. P. Jouppi, C. Young, N. Patil, D. Patterson, G. Agrawal, R. Bajwa, S. Bates, S. Bhatia, N. Boden, A. Borchers *et al.*, "In-datacenter performance analysis of a tensor processing unit," in *Proceedings of the 44th Annual International Symposium on Computer Architecture*, 2017, pp. 1–12.

- [11] A. Silva, F. Monticone, G. Castaldi, V. Galdi, A. Alù, and N. Engheta, "Performing mathematical operations with metamaterials," *Science*, vol. 343, no. 6167, pp. 160–163, 2014.
- [12] F. Zangeneh-Nejad, D. L. Sounas, A. Alù, and R. Fleury, "Analogue computing with metamaterials," *Nature Reviews Materials*, pp. 1–19, 2020.
- [13] A. Pors, M. G. Nielsen, and S. I. Bozhevolnyi, "Analog computing using reflective plasmonic metasurfaces," *Nano letters*, vol. 15, no. 1, pp. 791–797, 2015.
- [14] T. Zhu, Y. Zhou, Y. Lou, H. Ye, M. Qiu, Z. Ruan, and S. Fan, "Plasmonic computing of spatial differentiation," *Nature communications*, vol. 8, p. 15391, 2017.
- [15] H. Kwon, D. Sounas, A. Cordaro, A. Polman, and A. Alù, "Nonlocal metasurfaces for optical signal processing," *Physical review letters*, vol. 121, no. 17, p. 173004, 2018.
- [16] J. Zhou, H. Qian, C.-F. Chen, J. Zhao, G. Li, Q. Wu, H. Luo, S. Wen, and Z. Liu, "Optical edge detection based on high-efficiency dielectric metasurface," *Proceedings of the National Academy of Sciences*, vol. 116, no. 23, pp. 11 137–11 140, 2019.
- [17] H. Kwon, A. Cordaro, D. Sounas, A. Polman, and A. Alu, "Dual-polarization analog 2d image processing with nonlocal metasurfaces," *ACS Photonics*, 2020.
- [18] A. Youssefi, F. Zangeneh-Nejad, S. Abdollahramezani, and A. Khavasi, "Analog computing by brewster effect," *Optics letters*, vol. 41, no. 15, pp. 3467–3470, 2016.
- [19] D. A. Bykov, L. L. Doskolovich, A. A. Morozov, V. V. Podlipnov, E. A. Bezus, P. Verma, and V. A. Soifer, "First-order optical spatial differentiator based on a guided-mode resonant grating," *Optics express*, vol. 26, no. 8, pp. 10997–11 006, 2018.
- [20] T. Zhu, Y. Lou, Y. Zhou, J. Zhang, J. Huang, Y. Li, H. Luo, S. Wen, S. Zhu, Q. Gong *et al.*, "Generalized spatial differentiation from the spin hall effect of light and its application in image processing of edge detection," *Physical Review Applied*, vol. 11, no. 3, p. 034043, 2019.
- [21] C. Guo, M. Xiao, M. Minkov, Y. Shi, and S. Fan, "Photonic crystal slab laplace operator for image differentiation," *Optica*, vol. 5, no. 3, pp. 251–256, 2018.
- [22] N. M. Estakhri, B. Edwards, and N. Engheta, "Inverse-designed metasurfaces that solve equations," *Science*, vol. 363, no. 6433, pp. 1333–1338, 2019.
- [23] F. Zangeneh-Nejad and R. Fleury, "Topological analog signal processing," *Nature communications*, vol. 10, no. 1, pp. 1–10, 2019.
- [24] Y. Zhou, W. Wu, R. Chen, W. Chen, R. Chen, and Y. Ma, "Analog optical spatial differentiators based on dielectric metasurfaces," *Advanced Optical Materials*, vol. 8, no. 4, p. 1901523, 2020.
- [25] S. Abdollahramezani, O. Hemmatyar, and A. Adibi, "Meta-optics for spatial optical analog computing," *Nanophotonics*, vol. 9, no. 13, pp. 4075–4095, 2020.
- [26] A. Abdolali, A. Momeni, H. Rajabalipanah, and K. Achouri, "Parallel integro-differential equation solving via multi-channel reciprocal bianisotropic metasurface augmented by normal susceptibilities," *New Journal of Physics*, vol. 21, no. 11, p. 113048, 2019.
- [27] L. Wan, D. Pan, S. Yang, W. Zhang, A. A. Potapov, X. Wu, W. Liu, T. Feng, and Z. Li, "Optical analog computing of spatial differentiation and edge detection with dielectric metasurfaces," *Optics Letters*, vol. 45, no. 7, pp. 2070–2073, 2020.
- [28] Y. Zhou, H. Zheng, I. I. Kravchenko, and J. Valentine, "Flat optics for image differentiation," *Nature Photonics*, vol. 14, no. 5, pp. 316–323, 2020.
- [29] A. Momeni, H. Rajabalipanah, A. Abdolali, and K. Achouri, "Generalized optical signal processing based on multioperator metasurfaces synthesized by susceptibility tensors," *Physical Review Applied*, vol. 11, no. 6, p. 064042, 2019.
- [30] T. Davis, F. Eftekhari, D. Gómez, and A. Roberts, "Metasurfaces with asymmetric optical transfer functions for optical signal processing," *Physical review letters*, vol. 123, no. 1, p. 013901, 2019.
- [31] A. Babae, A. Momeni, A. Abdolali, and R. Fleury, "Parallel analog computing based on a 2×2 multiple-input multiple-output metasurface processor with asymmetric response," *Physical Review Applied*, vol. 15, no. 4, p. 044015, 2021.
- [32] A. Babae, A. Momeni, M. M. Moeini, R. Fleury, and A. Abdolali, "Parallel optical spatial signal processing based on 2×2 mimo computational metasurface," in *2020 Fourteenth International Congress on Artificial Materials for Novel Wave Phenomena (Metamaterials)*. IEEE, pp. 195–197.
- [33] A. Momeni, M. Safari, A. Abdolali, N. P. Kherani, and R. Fleury, "Asymmetric metal-dielectric metacylinders and their potential applications from engineering scattering patterns to spatial optical signal processing," *Physical Review Applied*, vol. 15, no. 3, p. 034010, 2021.
- [34] K. Achouri and O. J. Martin, "Angular scattering properties of metasurfaces," *IEEE Transactions on Antennas and Propagation*, vol. 68, no. 1, pp. 432–442, 2019.
- [35] T. Niemi, A. O. Karilainen, and S. A. Tretyakov, "Synthesis of polarization transformers," *IEEE Transactions on Antennas and Propagation*, vol. 61, no. 6, pp. 3102–3111, 2013.
- [36] E. F. Kuester, M. A. Mohamed, M. Piket-May, and C. L. Holloway, "Averaged transition conditions for electromagnetic fields at a metafilm," *IEEE Transactions on Antennas and Propagation*, vol. 51, no. 10, pp. 2641–2651, 2003.
- [37] C. L. Holloway, E. F. Kuester, J. A. Gordon, J. O'Hara, J. Booth, and D. R. Smith, "An overview of the theory and applications of metasurfaces: The two-dimensional equivalents of metamaterials," *IEEE Antennas and Propagation Magazine*, vol. 54, no. 2, pp. 10–35, 2012.
- [38] A. Arbabi, E. Arbabi, Y. Horie, S. M. Kamali, and A. Faraon, "Planar metasurface retroreflector," *Nature Photonics*, vol. 11, no. 7, p. 415, 2017.
- [39] A. Momeni, K. Rouhi, H. Rajabalipanah, and A. Abdolali, "An information theory-inspired strategy for design of re-programmable encrypted graphene-based coding metasurfaces at terahertz frequencies," *Scientific reports*, vol. 8, no. 1, pp. 1–13, 2018.
- [40] K. Rouhi, H. Rajabalipanah, and A. Abdolali, "Real-time and broadband terahertz wave scattering manipulation via polarization-insensitive conformal graphene-based coding metasurfaces," *Annalen der Physik*, vol. 530, no. 4, p. 1700310, 2018.
- [41] M. Kiani, M. Tayarani, A. Momeni, H. Rajabalipanah, and A. Abdolali, "Self-biased tri-state power-multiplexed digital metasurface operating at microwave frequencies," *Optics Express*, vol. 28, no. 4, pp. 5410–5422, 2020.
- [42] M. Kiani, A. Momeni, M. Tayarani, and C. Ding, "Spatial wave control using a self-biased nonlinear metasurface at microwave frequencies," *Optics Express*, vol. 28, no. 23, pp. 35 128–35 142, 2020.
- [43] H. Rajabalipanah, A. Abdolali, J. Shabanpour, A. Momeni, and A. Chel-davi, "Asymmetric spatial power dividers using phase-amplitude metasurfaces driven by huygens principle," *ACS omega*, vol. 4, no. 10, pp. 14 340–14 352, 2019.
- [44] S. E. Hosseininejad, K. Rouhi, M. Neshat, A. Cabellos-Aparicio, S. Abadal, and E. Alarcón, "Digital metasurface based on graphene: An application to beam steering in terahertz plasmonic antennas," *IEEE Transactions on Nanotechnology*, vol. 18, pp. 734–746, 2019.
- [45] S. E. Hosseininejad, K. Rouhi, M. Neshat, R. Faraji-Dana, A. Cabellos-Aparicio, S. Abadal, and E. Alarcón, "Reprogrammable graphene-based metasurface mirror with adaptive focal point for thz imaging," *Scientific reports*, vol. 9, no. 1, pp. 1–9, 2019.
- [46] R. Kargar, K. Rouhi, and A. Abdolali, "Reprogrammable multifocal thz metalens based on metal-insulator transition of vo2-assisted digital metasurface," *Optics Communications*, vol. 462, p. 125331, 2020.
- [47] C. Pfeiffer and A. Grbic, "Metamaterial huygens' surfaces: tailoring wave fronts with reflectionless sheets," *Physical review letters*, vol. 110, no. 19, p. 197401, 2013.
- [48] M. Selvanayagam and G. V. Eleftheriades, "Circuit modeling of huygens surfaces," *IEEE Antennas and Wireless Propagation Letters*, vol. 12, pp. 1642–1645, 2013.
- [49] K. Achouri, M. A. Salem, and C. Caloz, "General metasurface synthesis based on susceptibility tensors," *IEEE Transactions on Antennas and Propagation*, vol. 63, no. 7, pp. 2977–2991, 2015.
- [50] K. Achouri and C. Caloz, "Design, concepts, and applications of electromagnetic metasurfaces," *Nanophotonics*, vol. 7, no. 6, pp. 1095–1116, 2018.
- [51] M. Yazdi and M. Albooyeh, "Analysis of metasurfaces at oblique incidence," *IEEE Transactions on Antennas and Propagation*, vol. 65, no. 5, pp. 2397–2404, 2017.
- [52] M. Albooyeh, S. Tretyakov, and C. Simovski, "Electromagnetic characterization of bianisotropic metasurfaces on refractive substrates: General theoretical framework," *Annalen der Physik*, vol. 528, no. 9–10, pp. 721–737, 2016.
- [53] M. Safari, A. Momeni, A. Abdolali, and N. Kherani, "Electric dipole-free meta-cylinders," in *2019 44th International Conference on Infrared, Millimeter, and Terahertz Waves (IRMMW-THz)*. IEEE, 2019, pp. 1–2.
- [54] S. Tretyakov, *Analytical modeling in applied electromagnetics*. Artech House, 2003.
- [55] A. Serdiukov, I. Semchenko, S. Tertyakov, and A. Sihvola, *Electromagnetics of bi-anisotropic materials-Theory and Application*. Gordon and Breach science publishers, 2001, vol. 11.

- [56] E. D. Palik and G. Ghosh, *Electronic handbook of optical constants of solids: User Guide*. Academic Press, 1999.
- [57] M. Yazdi and N. Komjani, "Polarizability calculation of arbitrary individual scatterers, scatterers in arrays, and substrated scatterers," *JOSA B*, vol. 33, no. 3, pp. 491–500, 2016.
- [58] D. L. Sounas and A. Alù, "Fundamental bounds on the operation of fano nonlinear isolators," *Physical Review B*, vol. 97, no. 11, p. 115431, 2018.